MDPI

Article

Spatial Prediction of Diameter Distributions for the Alpine Protection Forests in Ebensee, Austria, Using ALS/PLS and Spatial Distributional Regression Models

Arne Nothdurft [1,*], Andreas Tockner [1], Sarah Witzmann [1], Christoph Gollob [1], Tim Ritter [1], Ralf Kraßnitzer [1], Karl Stampfer [2] and Andrew O. Finley [3]

1   Institute of Forest Growth, Department of Forest and Soil Sciences, University of Natural Resources and Life Sciences, Vienna (BOKU), Peter-Jordan-Str. 82, 1190 Vienna, Austria; andreas.tockner@boku.ac.at (A.T.); sarah.witzmann@boku.ac.at (S.W.); christoph.gollob@boku.ac.at (C.G.); tim.ritter@boku.ac.at (T.R.); ralf.krassnitzer@boku.ac.at (R.K.)
2   Institute of Forest Engineering, Department of Forest and Soil Sciences, University of Natural Resources and Life Sciences, Vienna (BOKU), Peter-Jordan-Str. 82, 1190 Vienna, Austria; karl.stampfer@boku.ac.at
3   Department of Forestry, Michigan State University, Natural Resources Building, East Lansing, MI 48824-1222, USA; finleya@msu.edu
*   Correspondence: arne.nothdurft@boku.ac.at

Abstract: A novel Bayesian spatial distributional regression model is presented to predict forest structural diversity in terms of the distributions of the stem diameter at breast height (DBH) in the protection forests in Ebensee, Austria. The distributional regression approach overcomes the limitations and uncertainties of traditional regression modeling, in which the conditional mean of the response is regressed against explanatory variables. The distributional regression addresses the complete conditional response distribution, instead. In total 36,338 sample trees were measured via a handheld mobile personal laser scanning system (PLS) on 273 sample plots each having a 20 m radius. Recent airborne laser scanning (ALS) data were used to derive regression covariates from the normalized digital vegetation height model (DVHM) and the digital terrain model (DTM). Candidate models were constructed that differed in their linear predictors of the two gamma distribution parameters. In the distributional regression approach, covariates can enter the model in a flexible form, such as via nonlinear smooth curves, cyclic smooths, or spatial effects. Supported by Bayesian diagnostics DIC and WAIC, nonlinear smoothing splines outperformed linear parametric slope coefficients, and the best implementation of spatial structured effects was achieved by a Gaussian process smooth. Model fitting and posterior parameter inference was achieved by using full Bayesian methodology and MCMC sampling algorithms implemented in the R-package BAMLSS. With BAMLSS, spatial interval predictions of the DBH distribution at any new geo-locations were enabled via straightforward access to the posterior predictive distributions of the model terms and by offering simple plug-in solutions for new covariate values. A cross-validation analysis validated the robustness of the proposed method's parameter estimation and out-of-sample prediction. Spatial predictions of stem count proportions per DBH classes revealed that regeneration of smaller trees was lacking in certain areas of the protection forest landscape. Therefore, the intensity of final felling needs to be increased to reduce shading from the dense, overmature shelter trees and to promote sunlight for the young regeneration trees.

Keywords: protection forest; Bayesian regression model; spatial regression model; distributional regression; diameter distribution modeling

1. Introduction

The forests of the Alps provide a wide range of ecosystem services. In addition to offering wood production and a unique habitat for a diverse set of species, these forests

protect people, buildings, and infrastructure from natural hazards such as snow avalanches, rockfalls, and mudslides [1]. Forests that protect human infrastructure are declared as "protection forests", often through a public authority's formal decree. In Austria, between 2009 and 2015, there were 20–70 severe rockfall events per year, resulting in 10 human injuries and damage to settlement areas and infrastructure [2]. Given its mountains terrain, ~15.7% (615,852 hectares, ha) of Austria's total forest area offer some level of protective function [3].

In an in situ rockfall experiment, Ref. [4] showed forest cover significantly reduced velocity, rebound height, residual hazard of rockfall, and depending on the quality and quantity of the forest structure, the number of rocks involved in a rockfall could be reduced by 64%. To a large degree, the protective effect of a forest is a function of the forest's vertical and horizontal structure. Specifically, relevant structural measures are stem density, tree size (i.e., diameter), and patch size (see, e.g., [1] and other references therein). To assess hazard risk and support the decision making in forest management activities, Ref. [5] uses computer simulation models informed with spatially explicit forest structural summary inputs. These forest structure inputs were traditionally derived from aerial image analysis [6]. More recently, however, laser imaging detection and ranging (LiDAR) data are being used to support forest inventories [7], and offer improved accuracy and efficiency through automation for mapping forest structures [8]. As demonstrated in [9], airborne LiDAR data can even be utilized to segment individual trees and measure their diameters.

Mean tree diameter and total stem count are often inadequate at characterizing forest structure, especially for structurally diverse settings. Building structural diversity through silvicultural treatments is a common management objective that has been shown to enhance biological diversity, carbon storage, and possibly climate resilience [10–12]. This desired structural diversity is often produced by "plentering", a highly intensive silvicultural prescription designed to move homogeneous stands to an uneven age structure with stratified crown layering [13]. The characterization of such structurally diverse forests is best approached through the use of more detailed summaries of potentially complex size-class distributions, which provide a more nuanced understanding of the forest's structure. The distribution of tree diameters is not only relevant for the management of forest ecosystems, but can also serve as an indicator of the structural diversity and of the quality of ecosystem services provided in urban regions [14].

Characterizing size-class distributions has traditionally been performed using either a parameter prediction model (PPM) or a parameter recovery model (PRM) approach [15]. In PPM, a probability density function (pdf) is chosen to characterize the size-distribution (e.g., diameter distribution), and the pdf parameters are then estimated separately for each sample plot. Finally, the parameter estimates are regressed against covariates via regression analysis. Using these regression equations with new values of the covariates achieves the final pdf parameter predictions for independent sample plots [16]. In PRM, theoretical moments of the pdf, e.g., the mean and dispersion parameters, are expressed dependent on the pdf parameters. In these equations, the theoretical moments are then replaced by their sample estimates. For a pdf with k parameters, a set of k equations is finally solved to achieve the pdf parameter estimates.

The PRM is often used to avoid confounding problems, which can occur with PPM, as similar pdfs can be achieved with different parameter combinations, making it difficult to find unambiguously meaningful covariates. As consequence, the PPM equations can usually explain only a little of the variation in the parameters and typically have a low R^2. A shortcoming of the traditional PPM and PRM approaches to modeling tree size distributions is that they require separate model steps—estimating size distribution parameters happens separately from the regression used to explain variability in those parameters. This can easily produce ill-behaved prognoses of diameter distributions when new covariate data are used. To make future predictions of diameter distributions more reliable and accommodate temporal dependence among repeat measurements, a bivariate distribution modeling was demonstrated in [16]. Ref. [17] proposed a non-parametric Bayesian approach to

estimate diameter distributions that modeled each diameter class using a Poisson regression informed using LiDAR covariates and random effects designed to accommodate correlation among diameter classes and across spatial locations. While highly flexible, their proposed approach was computationally demanding and required a greater degree of user input to choose appropriate prior distributions and assess model convergence.

Here, we demonstrate and assess a different inferential approach aimed at overcoming key limitations of previously proposed methods for characterizing size-class distributions. Specifically, we apply recent advancements in *distributional regression* using generalized additive models that facilitate joint estimation of shape and scale parameters in parametric distributions. In particular, we use a *generalized additive models for location, scale, and shape* (GAMLSS)-based approach, proposed by [18]. In a series of papers, Refs. [19–22] extended the original maximum likelihood mode of inference for GAMLSS parameters to a Bayesian approach using Markov chain Monte Carlo (MCMC), referred to as *Bayesian additive models for location, scale, and shape* (BAMLSS). This Bayesian approach accommodate a richer set of models and uncertainty quantification. Many proposed BAMLSS features have been made available in user-friendly software [23].

Unlike within classical regression models, where the conditional mean of the response is regressed against covariates, distributional regression addresses the complete conditional response distribution, in that each distribution parameter is modeled in terms of covariates and, potentially, random effects. Compared to maximum-likelihood-based GAMLSS, the BAMLSS distributional regression supports a wider selection of distribution families, for which the parameters are not necessarily directly related to the location, scale, and shape of the given distribution but can form these measures indirectly via functional relationships. Ref. [24] offers an excellent review of distributional regression approaches including GAMLSS (and its Bayesian extensions) and the traditionally more conspicuous quantile regression. The review underscores key advantages to GAMLSS approaches with regard to modeling distribution parameters using versatile additive structure, nonlinear functions, varying coefficients, and spatially and temporally structured random effects.

In this paper, GAMLSS spatial distributional regression models are used to quantify forest structural diversity based on stand-level DBH distributions in a protection forest landscape near Ebensee, Austria. Sample plot data were collected using a handheld mobile personal laser scanning (PLS) and processed using automated software routines. Regression covariates were derived from a digital vegetation height model (DVHM) and a digital terrain model (DTM) provided by recent airborne laser scanning (ALS) campaigns.

2. Materials and Methods

2.1. Study Region and Model Data

The study area was located in the southern region of the federal state of Upper Austria, near the village of Ebensee, and covers an area south of Traunsee lake (Figure 1). The forest district Ebensee had a total area of 4898 hectares (ha) and was partitioned into $Q = 1237$ forest stands. The average stand size was 3.96 ha, the minimum 0.14 ha, the median 2.33 ha, and the maximum 89.99 ha.

Forest inventory data were collected on $n = 273$ sample plots, which were spatially aligned in a regular 400 m × 400 m grid (Figure 1). Plot measurements were collected using a handheld mobile PLS GeoSLAM ZEB Horizon (GeoSLAM Ltd., Nottingham, UK). The 180 plots in the study area's eastern half were scanned in autumn 2021, and the remaining 93 plots, in the western half, were scanned in spring 2023. Position, diameter at breast height (DBH), and height for the approximately 36,338 measurement trees were derived from 3D point clouds collected on each 20 m radius plot centered on the n grid locations using fully automated routines detailed in [25–29]. Stem volume was calculated using a traditional stem-form function [30]. The mean DBH of the measured trees was 14.6 cm, the standard deviation (SD) was 10.6, the minimum was equal to the pre-defined 5 cm threshold, and the maximum DBH was 92.4 cm. For each plot, the growing stock timber volume (GSV) was expressed in m^3/ha (i.e., computed as the sum of tree volume scaled

by the 7.958 fixed-area plot tree expansion factor). The mean GSV of the sample plots was $259.6 \, \text{m}^3/\text{ha}$, the SD was $177.9 \, \text{m}^3/\text{ha}$, and the minimum and maximum were $0.6 \, \text{m}^3/\text{ha}$ and $980.7 \, \text{m}^3/\text{ha}$, respectively.
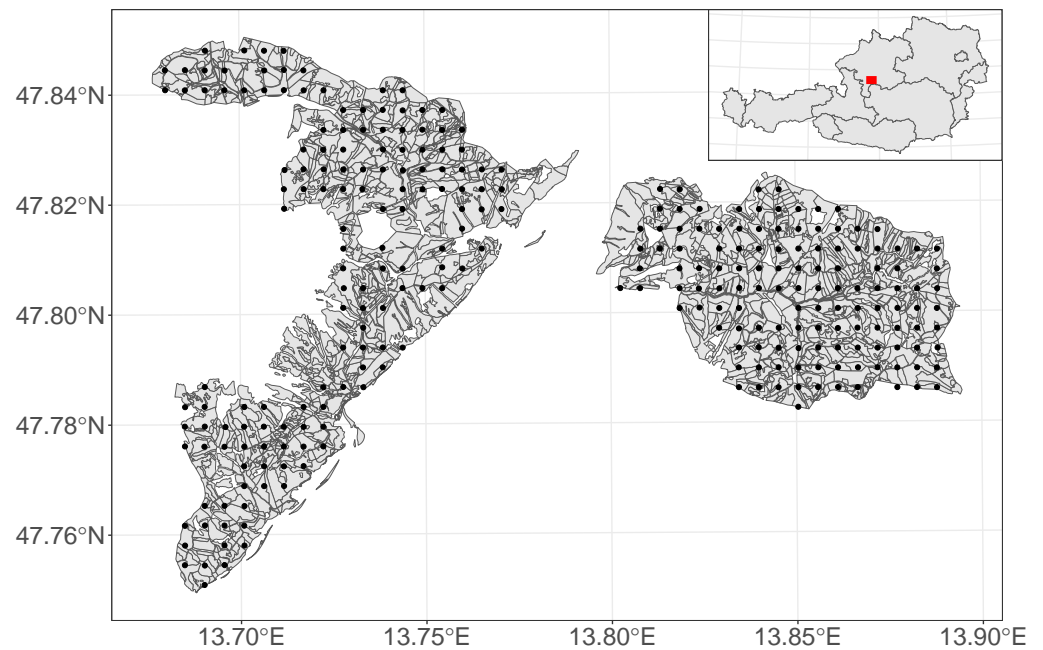
Figure 1. Schematic map of the extent of the Ebensee forest district in Austria and the locations of 273 sample points.

The federal state of Upper Austria provided open access to a DTM and a DSM via the open data platform https://data.ooe.gv.at [31,32]; both were available as $0.5 \, \text{m} \times 0.5 \, \text{m}$ resolution grids in the tagged image file format. The DTM and DSM were processed from ALS data obtained in different flight campaigns conducted over the past several years. For 84% of the total forest district area, the ALS data were collected in 2021, for 11% in 2019, and for the remaining 5% in 2017. A normalized DVHM was computed by subtracting the DTM from the DSM.

2.2. Model Construction

A distributional regression model was built for the DBH distributions observed at the n PLS forest inventory plots with the model form

$$\boldsymbol{y}_i | \boldsymbol{x}_i \sim \mathcal{D}(\vartheta_1(\boldsymbol{x}_i), \ldots, \vartheta_K(\boldsymbol{x}_i)), \tag{1}$$

where $\boldsymbol{y}_i$ is the DBH distribution vector at the ith plot, and $\mathcal{D}$ is a parametric density distribution function with parameters $\vartheta_1(\boldsymbol{x}_i), \ldots, \vartheta_K(\boldsymbol{x}_i)$ that depend on a set of plot specific covariates $\boldsymbol{x}_i$.

The parameters are typically not directly generated by a regression predictor; rather, they are often derived through a monotonically increasing response function, which maps the predictor $\eta_i^{\vartheta_l}$ to the lth parameter via

$$\vartheta_{il} = h_l(\eta_i^{\vartheta_l}) \, . \tag{2}$$

Assuming monotony and inverting the response function via the link function $g_l(\cdot)$ achieves the parameter predictor

$$\eta_i^{\vartheta_l} = h_l^{-1}(\vartheta_{il}) = g_l(\vartheta_{il}) \, . \tag{3}$$

The vector of covariates $x_i' = (z_i', v_i', s_i')$ optionally contains measures z_i' having a linear effect, v_i' having nonlinear effects, and s_i representing generic geo-locations. Hence, the structured additive predictor becomes

$$\eta_i^{\vartheta_l} = z_i' \beta^{\vartheta_l} + \sum_{j=1}^{J_l} f_j^{\vartheta_l}(v_i) + f_{\text{geo}}^{\vartheta_l}(s_i) \, , \tag{4}$$

and is composed of linear covariate effects with parameters β^{ϑ_l} in the first summand, smooth nonlinear functions $f_j^{\vartheta_l}(\cdot)$ in the second summand, and a spatial effect $f_{\text{geo}}^{\vartheta_l}(\cdot)$ at geo-locations s_i in the third summand.

Distributional regression models were constructed with the gamma distribution as the proper candidate for $\mathcal{D}$. Trials were also made with the Weibull distribution, but the Weibull distribution proved less flexible than the gamma distribution. Following [33], the gamma distribution's probability density function (pdf) considered here is defined by

$$f_{\text{GA}}(y|\mu,\sigma) = \frac{y^{1/\sigma^2 - 1} e^{-y/(\sigma^2\mu)}}{(\sigma^2\mu)^{1/\sigma^2} \Gamma(1/\sigma^2)} \, , \tag{5}$$

for $y > 0$, and with $\mu > 0$ and $\sigma > 0$. Herein, $\text{E}(Y) = \mu$ and $\text{Var}(Y) = \sigma^2\mu^2$. Linear predictors (Equation (4)) were constructed for both parameters μ and σ.

The catalog of the possible covariates for z_i and v_i included summary statistics of the DVHM across the pixels per sample plot area, such as the mean vegetation height (MVH), its standard deviation (SDVH), and various percentiles of the distributions of the pixelated vegetation heights. In addition, topographic metrics were derived from the DTM, i.e., the elevation above sea level (ESL), and the average slope (SLO) and aspect (ASP) of the terrain. Finally, the geo-locations of the sample plot centroids were used to index a spatial Gaussian process (i.e., the $f_{\text{geo}}^{\vartheta_l}(s_i)$ summand in (4)).

Various candidate models were tested that differed in their complexity, especially in terms of smooth nonlinear models for the covariate effects versus simple linear parametric coefficients, and with respect to the presence/absence of a structured spatial effect.

The model fitting and subsequent prediction was performed within a Bayesian inferential framework and by using the R-package BAMLSS version 1.2-4 [22,23]. Smooth nonlinear covariate effects (second summand in Equation (4)) were consistently modeled with BAMLSS's default thin-plate regression splines [34], and the spatially structured effect for the continuously indexed sample plot location coordinates (third summand in Equation (4)) were alternatively represented by a spatial Gaussian process model or by a bivariate tensor product smooth. When a Gaussian process was chosen, a simplified form of the Matern covariance function was applied, according to suggestions by [35]. Parameter inference was derived from posterior distributions that were sampled via MCMC techniques. Computations were performed on a multi-core processor workstation. On 7 cores, 5000 iterations were computed per core. From each of the 7 chains, the first 2000 iterations were discarded as "burn-in", and from the remaining 3000 iterations every 10th sample was kept. This burn-in and thinning yielded approximately $M = 2100$ nearly independent MCMC samples upon which parameter and predictive posterior inference was based. The performances of the different candidate models were assessed by means of the deviance information criterion (DIC) [36] and two varieties of the widely applicable information criterion (WAIC1 and WAIC2) defined in [37]. For both, lower values of the DIC and WAIC indicate an improved model fit.

2.3. Model Validation

The best candidate model, in terms of the DIC and WAIC, was validated in a 10-fold cross-validation procedure. In this way, the total sample of $n = 273$ plots was randomly split into 10 lots, each having approximately the same size, $n/10$. In each of the 10 iterations, a different single lot was held back, and the model was fitted to the data from the remaining

9 lots. The posterior predictive distributions of the parametric and non-parametric model effects were then used to evaluate the posterior predictive distributions of μ and σ given the independent regressor variables from the withheld lot. Summaries of these predictive distributions were finally compared with their counterparts, which were derived from the full-data model fit.

2.4. Prediction

Our primary interest was in stem diameter distribution prediction for each of the 1237 forest stands delineated in Figure 1. For this purpose, the entire Ebensee forest district domain was partitioned into 35.5 m × 35.5 m squared prediction pixels, where each pixel's area equals that of the 20 m radius sample plot. For each of the prediction pixels, the same set of covariates was derived as was used in the candidate models. Then, given these prediction pixel covariate values and centroid coordinates, posterior predictive distribution samples were generated via composition sampling for each pixel's μ and σ, and subsequently, their gamma pdf-based stem diameter distribution.

To assess the protective function of the forest stands in terms of their structural diversity, forest practitioners from the Austrian Federal Forest Service were especially interested in the percentage shares of the stems that were allocated to broader diameter classes: (1) small (DBH < 25 cm), (2) intermediate (25 cm ≤ DBH ≤ 50 cm), and (3) large (DBH > 50 cm).

To produce such estimates, the gamma distribution function $F_{GA}(\cdot)$ was evaluated with the $\mu_{j,m}^{(q)}$ and $\sigma_{j,m}^{(q)}$ estimates from each posterior sample $m = 1, \ldots, M$ for each prediction pixel $j = 1, \ldots, J_q$ of the total J_q pixels within each forest stand, indexed by $q = 1, \ldots, 1237$ via (1) $P_{j,m}^{(q)}(\text{DBH} < 20\,\text{cm}) = F_{GA}(y = 20|\mu_{j,m}^{(q)}, \sigma_j^{(q)})$; (2) $P_{j,m}^{(q)}(20 \le \text{DBH} \le 45\,\text{cm}) = F_{GA}(y = 45|\mu_j^{(q)}, \sigma_j^{(q)}) - F_{GA}(y = 20|\mu_j^{(q)}, \sigma_j^{(q)})$; and (3) $P_{j,m}^{(q)}(\text{DBH} > 45\,\text{cm}) = 1 - F_{GA}(y = 45|\mu_j^{(q)}, \sigma_j^{(q)})$.

Complete posterior predictive distributions of the M aggregated estimates per forest stand were generated by an area-weighting through

$$P_m^{(q)}(\cdot) = \frac{1}{\sum_{j=1}^{J_q} a_j} \sum_{j=1}^{J_q} a_j P_{j,m}^{(q)}(\cdot) \,, \qquad (6)$$

with a_j being the non-constant area of pixel j that falls into stand q, and that might be reduced by stand border intersections.

3. Results
3.1. Candidate Models

In total, 15 candidate models were constructed that differed in their covariates and in their constructions of the linear predictors for the μ and σ parameters of the gamma distribution (Table 1). The covariate effects were either modeled through a linear trend that was represented by a single parametric slope coefficient, or via non-parametric smoothing splines. The effect of the terrain aspect (ASP) was throughout represented by a cyclic version of a cubic regression spline smooth. The spatially structured effects were either modeled by a bivariate tensor product smooth with the continuous x,y-coordinates of the sample plots, or alternatively, by a Gaussian process.

Table 1. Construction of the candidate models. Abbreviations of the covariates: MVH (mean vegetation height), SDVH (standard deviation of the vegetation height), PX (Xth percentile of the vegetation height distribution), ESL (elevation above sea level), SLO (average terrain slope), ASP (aspect of the terrain), and XY (geo-locations). "p" stands for a parametric effect and "s()" for a non-parametric smoothing spline. "s(cc)" indicates a cyclic version of a regression spline smooth. Spatially structured effects are either modeled by assuming a Gaussian process "s(gp)" or via a tensor product smooth "te". Diagnostics show the deviance information criterion (DIC), two calculation variants of the widely applicable information criterion (WAIC1, WAIC2), and the associated effective number of model parameters (edf, p1, p2). Lowest DIC and WAIC are in bold.

	m_1	m_2	m_3	m_4	m_5	m_6	m_7	m_8	m_9	m_10	m_11	m_12	m_13	m_14	m_15
MVH	p	s	s	s	s	p	p	s	s	s	s	s	s	s	s
SDVH	p	s	s	s	s	p	p	s	s	s	s	s	s	s	s
P2.5				p	s							p	p	s	s
P97.5				p	s							p	p	s	s
ESL	p	s	s	s	s	p	p	s	s	s	s	s	s	s	s
SLO			s	s	s					s	s	s	s	s	s
ASP			s(cc)	s(cc)	s(cc)					s(cc)	s(cc)	s(cc)	s(cc)	s(cc)	s(cc)
XY						s(gp)	te	s(gp)	te	s(gp)	te	s(gp)	te	s(gp)	te
DIC	231.268	229.278	228.321	228.087	227.304	230.008	230.235	228.347	228.460	227.577	227.630	227.214	227.236	**226.486**	226.526
edf	8.1	53.2	85.8	87.3	114.2	62.6	51.2	107.9	94.4	137.6	129.4	139.1	132.1	166.1	158.1
WAIC1	231.269	229.277	228.319	228.086	227.302	230.005	230.233	228.343	228.458	227.574	227.627	227.211	227.234	**226.484**	226.524
WAIC2	231.269	229.278	228.321	228.088	227.305	230.006	230.234	228.346	228.460	227.577	227.631	227.215	227.238	**226.489**	226.529
p1	8.4	52.7	83.9	85.7	112.2	60.0	49.7	104.3	91.9	134.5	126.9	135.9	129.9	163.8	156.6
p2	8.4	53.3	84.8	86.7	113.7	60.5	50.1	105.6	93.0	136.4	128.5	137.8	131.7	166.6	159.2

The distributional regression framework provided high flexibility and generally enabled different specifications of the linear predictors for both the μ and σ parameters of a single-distributional regression model. However, it was found that a unique specification of both linear predictors worked well throughout all candidate models. Consequently, the two linear predictors of the μ and σ parameters of each distributional regression model were constructed with the same set of covariates and by using the same model representations (parametric term vs. smoothing spline) for the respective covariate effects.

Comparisons of the model performances in terms of the DIC and two calculations of the WAIC suggested that smoothing splines were more useful than the parametric linear trends; see diagnostics in Table 1 for m_2 versus (vs.) m_1, m_5 vs. m_4, m_8 vs. m_6, m_9 vs. m_7, m_14 vs. m_12, and m_15 vs. m_13. Our findings indicated that a spatially structured effect consistently improved the model performance, although this was generally associated with an increased number of effective model parameters (edf, p1, p2); compare m_6 and m_7 vs. m_1, m_8 and m_9 vs. m_2, m_10 and m_11 vs. m_3, m_12 and m_13 vs. m_4, and m_14 and m_15 vs. m_5. When a spatially structured effect was considered, a Gaussian process was found to be a superior alternative to a tensor product smooth; compare m_6 vs. m_7, m_8 vs. m_9, m_10 vs. m_11, m_12 vs. m_13, and m_14 vs. m_15. Among all 15 candidate models, model m_14 had a marginally lower DIC and WAIC, and hence, was considered as the "best" and used for subsequent diameter distribution predictions.

3.2. Analysis and Inference of the Best Model

The effect curves of model m_14 (Figure 2) showed that the mean vegetation height (MVH) and elevation above sea level (ESL) had positive effects on μ and σ parameters. The slope of the terrain (SLO) as well as the 97.5th percentile of the pixelated vegetation height measures (P97.5) had almost strictly negative effects on μ and σ. The standard deviation of the vegetation height (SDMVH) had a strictly positive effect on μ. However, the effect of SDMVH on σ behaved ambiguously for values below 10, had a negative effect between 10 and 13, and acted positively for values greater than 13. The cyclic effect of the topographic aspect (ASP) on μ and σ had distinct local minima and maxima. The effect of the 2.5th percentile of the pixelated vegetation heights (P2.5) was indistinct for values less than 10 m, but for greater values, it had a positive effect on μ and on σ.

The quantile–quantile plot (qq-plot) in Figure 3 shows quantile residuals lay close to the bisecting line between -2 and 3. This indicates the gamma distributional assumptions are an accurate representation of the data, and that the distributional regression model m_14 was correctly specified.

For the model data of the 273 sample plots, the posterior mean estimates from the M MCMC samples of the μ parameter ranged between 2.93 and 35.62, and the 273 posterior mean estimates of the σ parameter lay between 0.43 and 3.1 (Figure 4). The correlation between the 273 posterior mean estimates for μ and σ was 0.42. The average relative standard deviation (SD%) of the μ estimates was 5.0%, and the σ estimates had an SD% of 7.2%.

Empirical histograms and posterior distributional predictions of the DBH distributions on the 273 model data sample plots are presented in Figures A1–A8 in the Appendix A. These figures show the distributional predictions fit very well to the empirical histograms across all sample plots.

To assess what influence the covariates simultaneously had on both distribution parameters μ and σ, the gamma density was evaluated under *ceteris paribus* conditions for grid values within the range of a single covariate, while the other covariates were kept fixed at their respective median values (Figure 5). As MVH acted positively on the expectation as well as on the variance in the gamma distribution, an increasing MVH flattened the density and shifted the mass towards higher DBH values. Similar effects occurred for increasing SDVH and ESL values. A completely opposite effect became obvious for an increasing P97.5. More complex and nonlinear effects on the DBH distribution were observed for SLO, ASP, and P2.5.
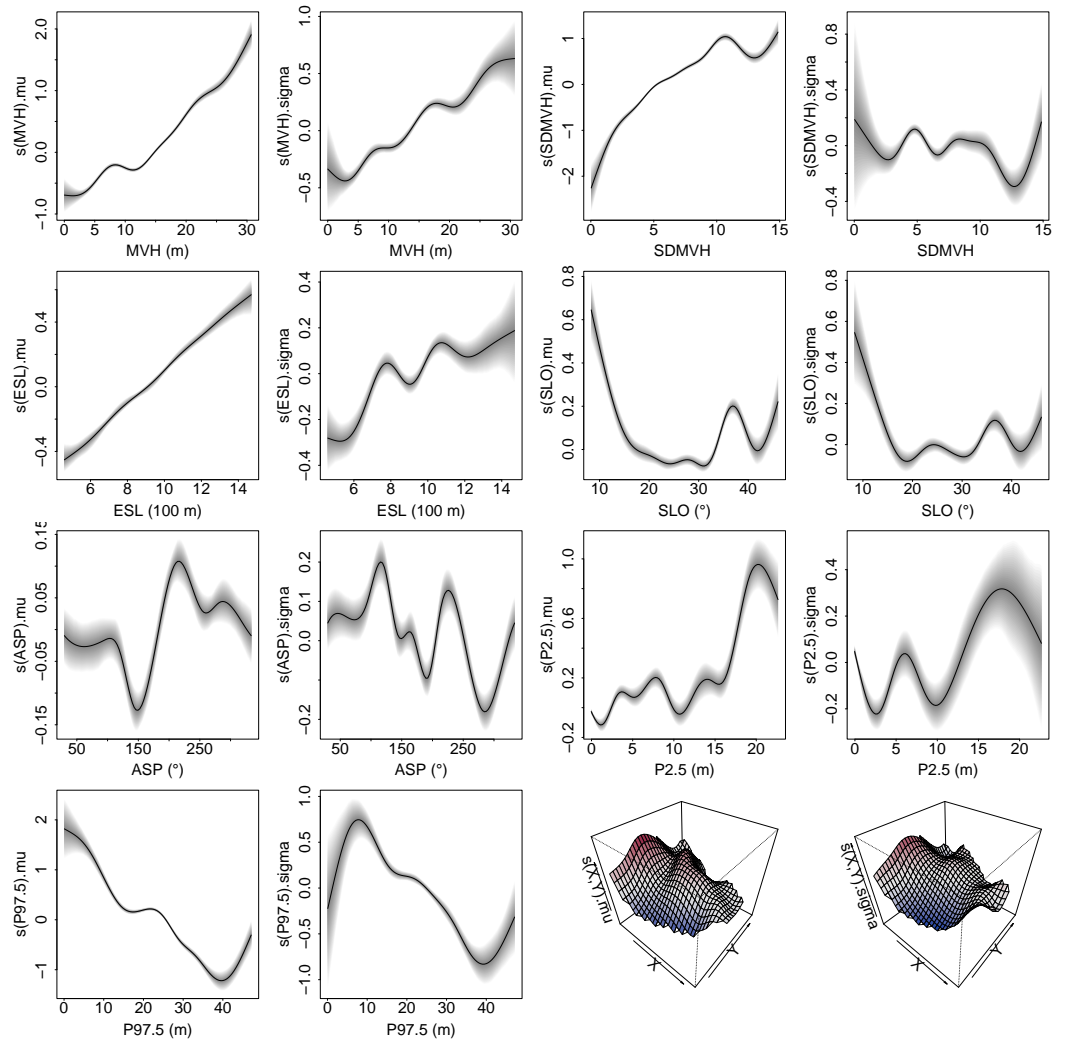
Figure 2. Effect curves and 95% credible intervals of the "best" model m_14. Covariate effects on μ are indicated by s($\cdot$).mu, and effects on σ by s($\cdot$).sigma.
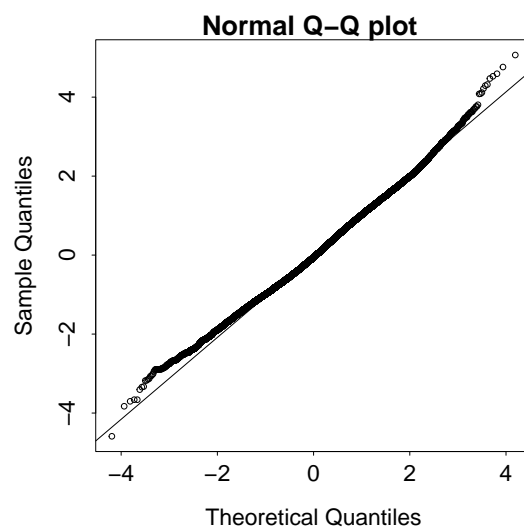
Figure 3. Quantile–quantile plot of the residuals from model m_14.
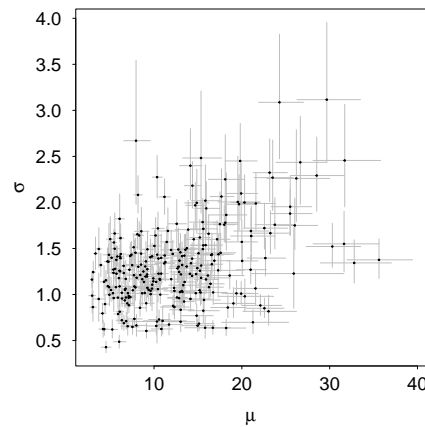
Figure 4. Posterior estimates of μ and σ for the model data from the 237 sample plots. The dots indicate the posterior mean, and the segments show 95% credible intervals.
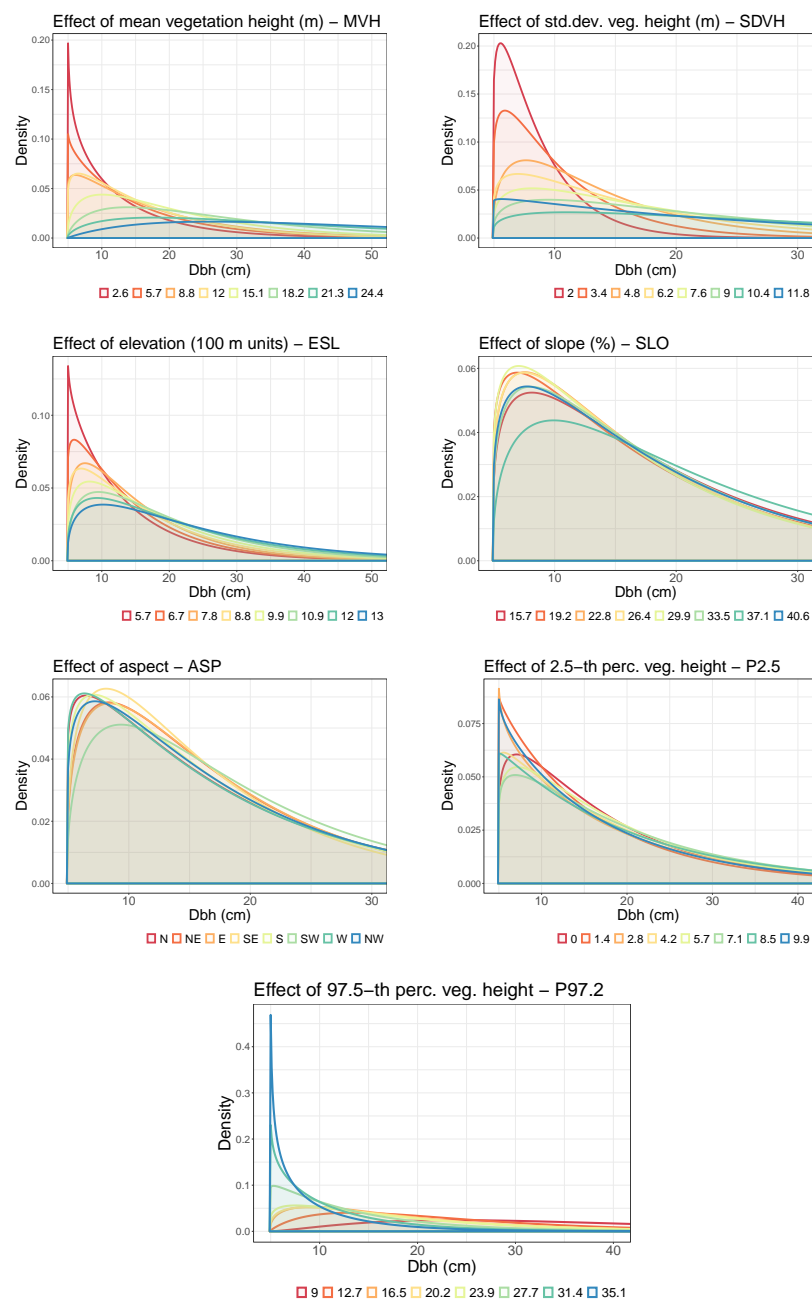
Figure 5. Visualization of the covariate effects on the DBH distribution.

The results from the 10-fold cross-validation showed that the independent posterior predictions of the μ and σ parameters were highly correlated with the predictions that were achieved by the model fit to the full dataset; see Figure 6. Despite only a few outliers, the correlation between the mean estimates of μ was 0.86, and the correlation was 0.81 for σ. Hence, the final model m_14 was robust, although the effect curves show some signs of "wiggliness".
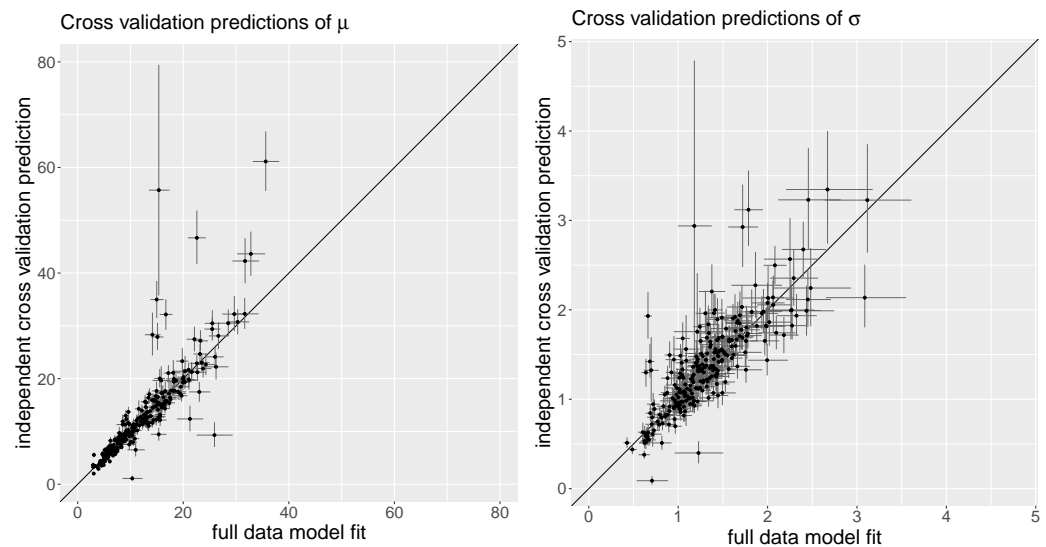
Figure 6. Comparison of the μ and σ posterior estimates from the 10-fold cross-validation against the posterior predictions with full-data model fits. Segments show 90% credible intervals.

3.3. Distributional Prediction

As noted previously, the Ebensee forest district domain was partitioned into 35.5 m × 35.5 m pixels. For each of these prediction pixels, covariate data were derived from the DVHM and the DSM in terms of the MVH, SDMVH, ESL, SLO, ASP, P2.5, P97.5, and the pixel centroid coordinates. The MCMC samples from the posterior parameter distributions for the covariate effects of model m_14 were then applied with these covariates to achieve posterior predictive distributions of μ and σ for each prediction pixel. Consequently, the gamma distribution was evaluated using these parameter estimates to produce predictions of stem count proportions that fall into the DBH classes specified in Section 2.4. Finally, an area-weighting scheme was applied to achieve aggregated predictions of these stem count proportions throughout all prediction pixels per forest stand. As demonstrated in Figure 7, the 95% credible intervals were relatively tight and the size class predictions became highly precise across all forest stands.

Maps of these size class predictions (Figure 8) revealed that smaller tree sizes were especially lacking in the central area of the Feuerkogel region located in the western part of the forest district Ebensee, while these stands also possessed a relatively high proportion of larger trees. As reported by the sample plot field crew, these sites were actually in a mature state, and establishment of natural regeneration was hindered by the dense shelter of larger mature trees. Appropriate silvicultural management activities are therefore needed to restore the protection function in this area. The size class predictions were relatively precise for both classification schemes and across all forest stands. The average standard deviation was only 0.85 percentage points, and the maximum was 9.6. The SD was less than 1.6 percentage points for 90% of the size class predictions, and 95% of the predictions had an SD less than 2 percentage points (Figure 9).
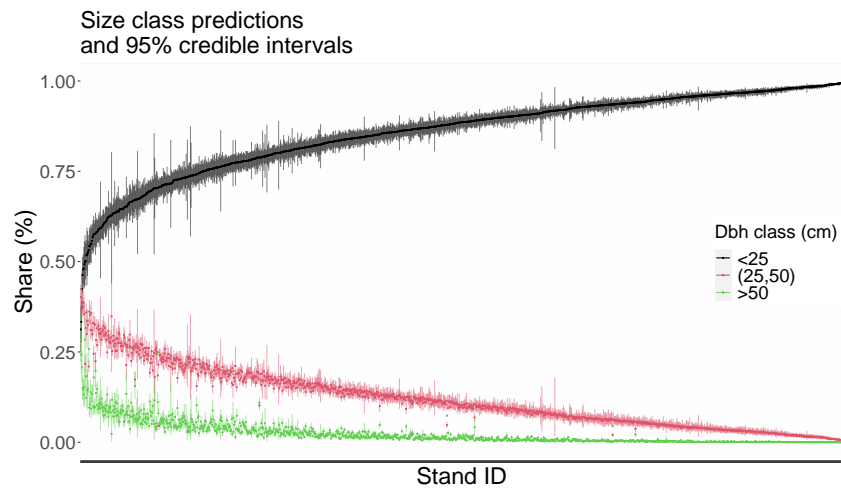
Figure 7. Predictions of DBH class allocations across the forest stands for the two classification variants.
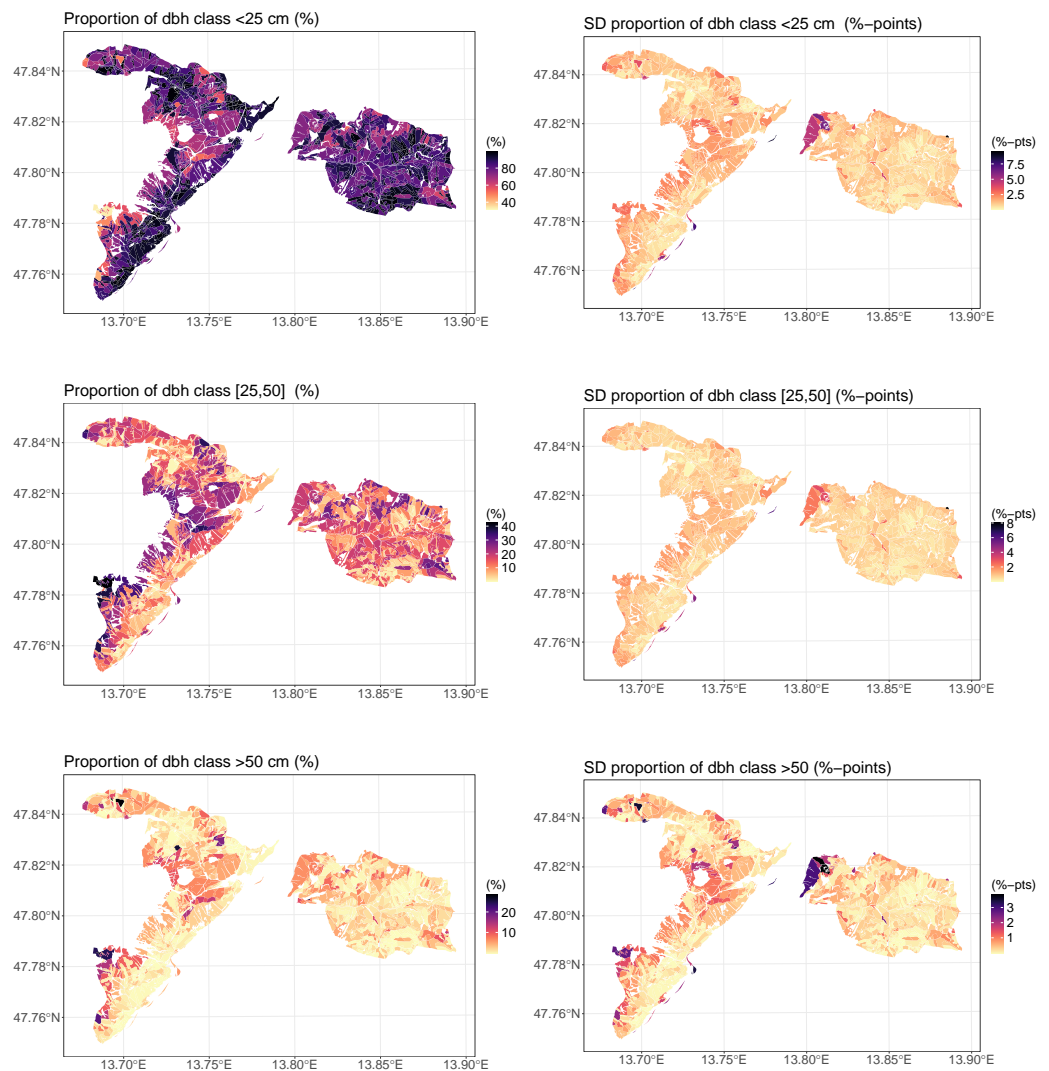
Figure 8. Spatial size class predictions (%) and standard deviation (% points) for the forest stands in the forest district Ebensee using the classification (1) small (DBH < 25 cm), (2) intermediate (25 cm ≤ DBH ≤ 50 cm), and (3) large (DBH > 50 cm).
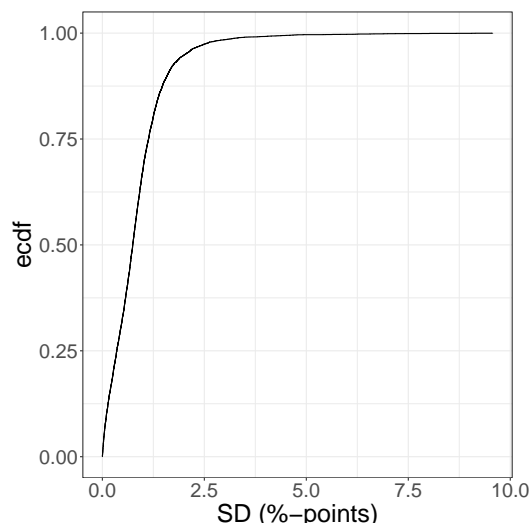
Figure 9. Empirical cumulative distribution function (ecdf) of the size-class prediction standard deviations (SDs).

4. Discussion

Posterior standard deviations of the DBH class predictions were low due to the spatially dense network of PLS sample points. There are some areas of higher uncertainty in the top corner of the eastern half of the district, which are characterized by irregular forests on steep slopes, and due to rock faces no PLS sample points could be captured. Also, the south-western ridge in the western half of the district, has higher errors, caused by missing points due to inaccessibility and generally rough terrain at high altitudes with less forest cover.

Spatially coherent diameter distribution predictions and subsequently derived probabilistic maps of meaningful size classes provided useful tools to support forest management decisions. In the Ebensee area, we found an overall high proportion of small-diameter trees, which are essential to sustain the protective function, especially in that steep terrain. Due to a dense forest road network in the forest district it is relatively easy to maintain forest regeneration. Nevertheless, some regions might need additional active management, especially in the central western half and in the center of the eastern half as well as in the south-eastern corner. Therefore, the intensity of final felling needs to be increased to reduce shading from the dense, overmature shelter trees and to promote sunlight for the young regeneration trees. Predictions of the diameter distribution alone are still insufficient to fully assess the forest's protective function, and of special interest would be an assessment of the structural change over time.

Our proposed methodology stands in stark contrast to the study of [38]. Whereas in [38] the mean forest-stand-level DBH was modeled within a generalized regression neural network, we have approached the complete conditional DBH distribution using a Bayesian distributional regression model. The proposed modeling framework is flexible and able to represent all the structural differences among the sample plots. However, forest stands could theoretically possess a layered structure with an understorey of younger and thinner trees growing under a shelter of older and thicker trees. These circumstances often result in a multimodal DBH distribution. Practically, such a structure could be modeled through a mixture of two or more different density functions. However, the methodology so far provided by the BAMLSS package is restricted to a single density and does not allow construction of composed mixture models. This limitation was practically irrelevant for our study, because none of the sample plots showed clear signs of a strict multimodal DBH distribution; compare Figures A1–A8 in the Appendix A.

In addition, any problems that could have been caused by BAMLSS's limitation to unimodal distributions were ameliorated by our approach to achieve the predictions at the forest stand level. Thereby, the forest stands were partitioned into smaller prediction pixels.

For each of the prediction pixels, the gamma distribution parameters were predicted, and the density was evaluated. The forest-stand-level prediction of the DBH distributions was finally achieved via an area-weighted aggregate of the pixel-level densities. In this way, the final prediction of the DBH distribution at stand level was no longer restricted to a unimodal parametric shape.

Forest inventory field work was conducted using a PLS to create "digital twins" of the vegetation and the terrain on a 20 m radius plot. The field work was very efficient, with approximately 12 min labor time per plot, including the set-up of the equipment and the scanning process. By using fully automated routines, 133 trees were measured on average per sample plot, with LiDAR-derived information on not only DBH, but also other parameters such as height and crown base. This is in contrast to the traditional forest inventory practice, in which measurements are conducted with optical and mechanical instruments. Because these instruments have high labor costs, traditional forest inventories use much smaller plot sizes than our 20 m radius plots, so that often not more than 10 trees are measured per plot. With such small sample sizes, the distributional regression modeling would have been hardly possible, and the novel PLS-supported forest inventory can be regarded as key to successful DBH distribution modeling and prediction.

In contrast to the proposed distributional regression framework, the traditional PRM approach is able to generate pdfs of stem diameters that lead to basal area sums, stem counts, and volume aggregates that correspond with the sample plot observations. Indeed, there is no guarantee that this likewise happens with the distributional regression approach. In this study, an approach was presented to model and predict stem diameter distributions in terms of a parametric probability density function. To produce a quantitative prediction of the absolute stem count per DBH class, a further estimate of the total stem count per area unit is needed. A possible approach to achieve such an estimate would be to couple the proposed spatial distribution regression model with an extra spatial spatial regression model that considers the tree count per hectare as response. An appropriate methodology for the spatial regression modeling of the growing stock timber volume per area unit is presented in [39] and could be adopted to model the number of trees per hectare. To date, high-density ALS data are available for the complete Ebensee forest district domain and will probably be maintained in the future, as the area is designated as a research zone and has been of particular interest to the Austrian Federal Forest Service. In future work, we will therefore also test an individual tree segmentation from the ALS canopy height model using a methodology implemented in the R-package lidR by [40,41] that provides a comparative approach to the spatial regression model of tree counts.

5. Conclusions

This study presented a method to estimate stem diameter distributions by linking PLS and ALS data in the protection forest landscape Ebensee. The Bayesian distributional regression framework was based on gamma distributions as implemented in the BAMLSS R-package. The gamma distribution's shape and scale parameters were modeled using linear predictors dependent on covariates from the PLS and ALS data. BAMLSS offered the modeling of nonlinear covariate effects by using penalized regression spline smoothers, which proved more favorable than linear parametric slope coefficients. Including spatially structured effects on both gamma parameters significantly enhanced the model performance. Thereby, the modeling of a spatial Gaussian process outperformed a bivariate tensor product smooth across the sample plot location coordinates.

A spatial wall-to-wall prediction of the gamma distribution was achieved by partitioning the entire domain into prediction pixels with an area equal to the sample plot. The DBH distributions were predicted at forest stand level via area-weighted aggregates of the evaluated posterior predictive densities.

The proposed model framework can be easily adopted to other tasks when information is required on forest structural diversity across broader forest landscapes. The latter aspect might be of special interest to forestry enterprises charged with protection forest manage-

ment. In such settings, estimating DBH distributions and other forest structure measures can inform management decisions focused on sustaining protective forest characteristics.

Appendix A

Figure A1. Histograms (grey bars) and posterior predictive distributions (red curves) of the DBH at the sample plots (plot id in title).
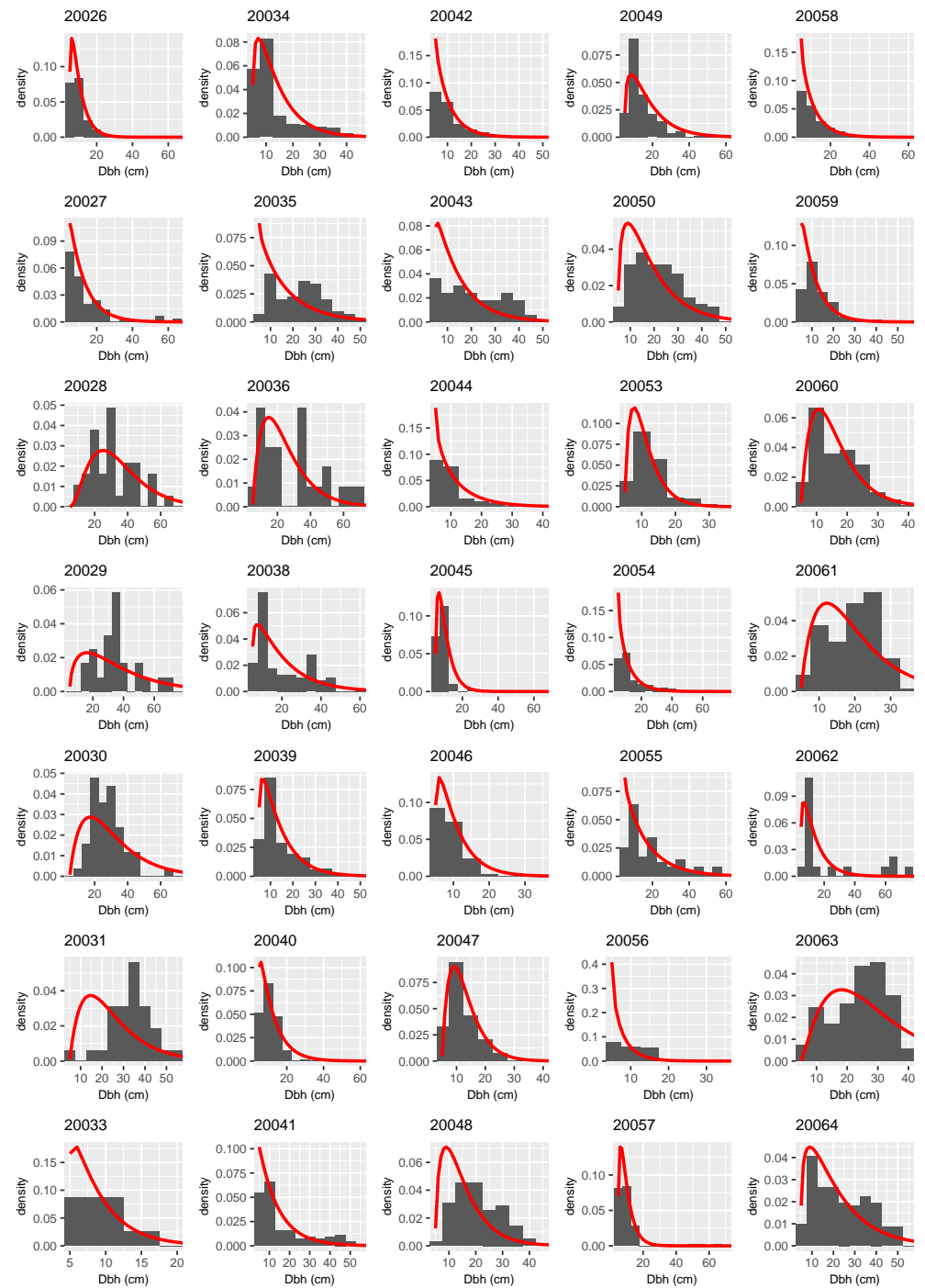
Figure A2. Histograms (grey bars) and posterior predictive distributions (red curves) of the DBH at the sample plots (plot id in title).
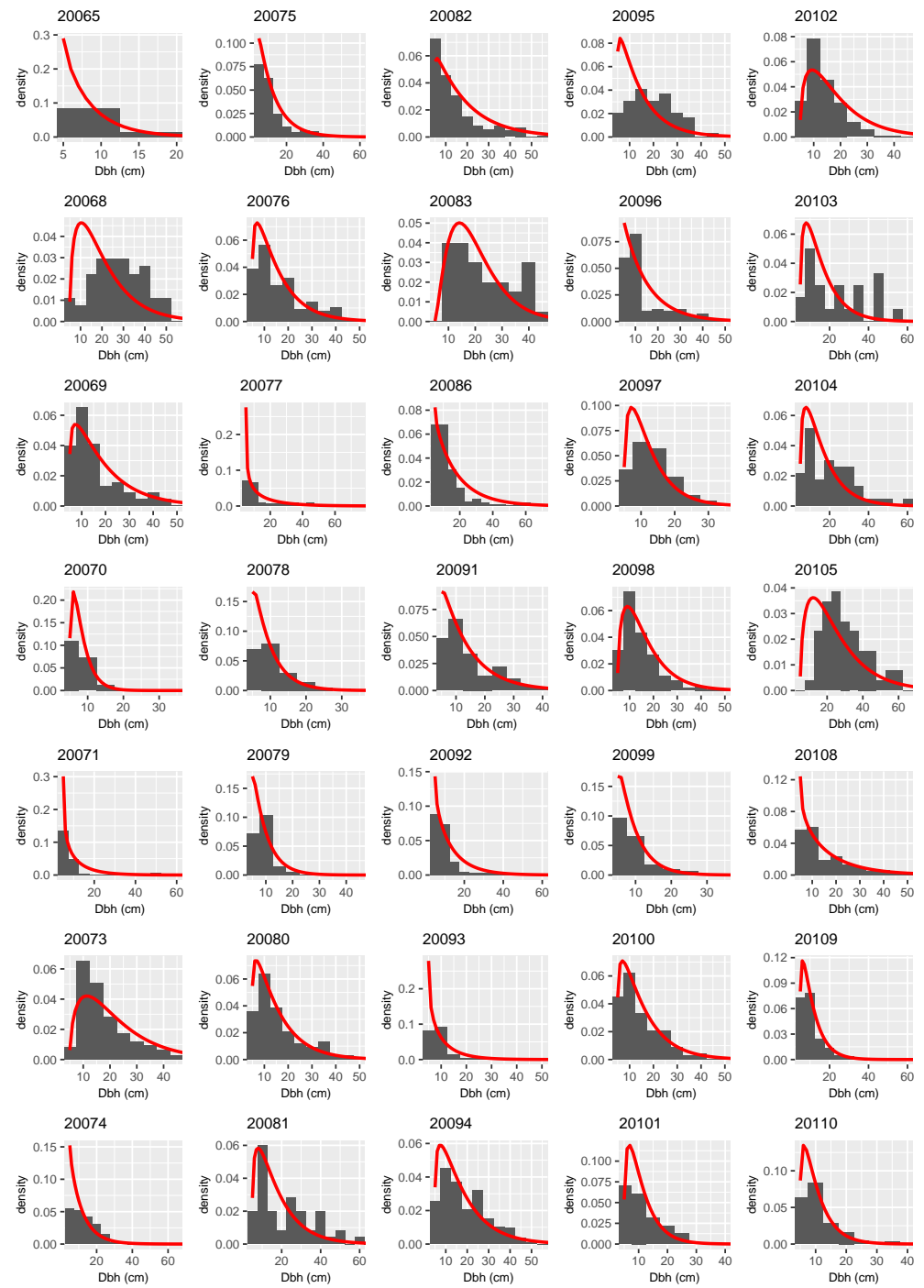
Figure A3. Histograms (grey bars) and posterior predictive distributions (red curves) of the DBH at the sample plots (plot id in title).
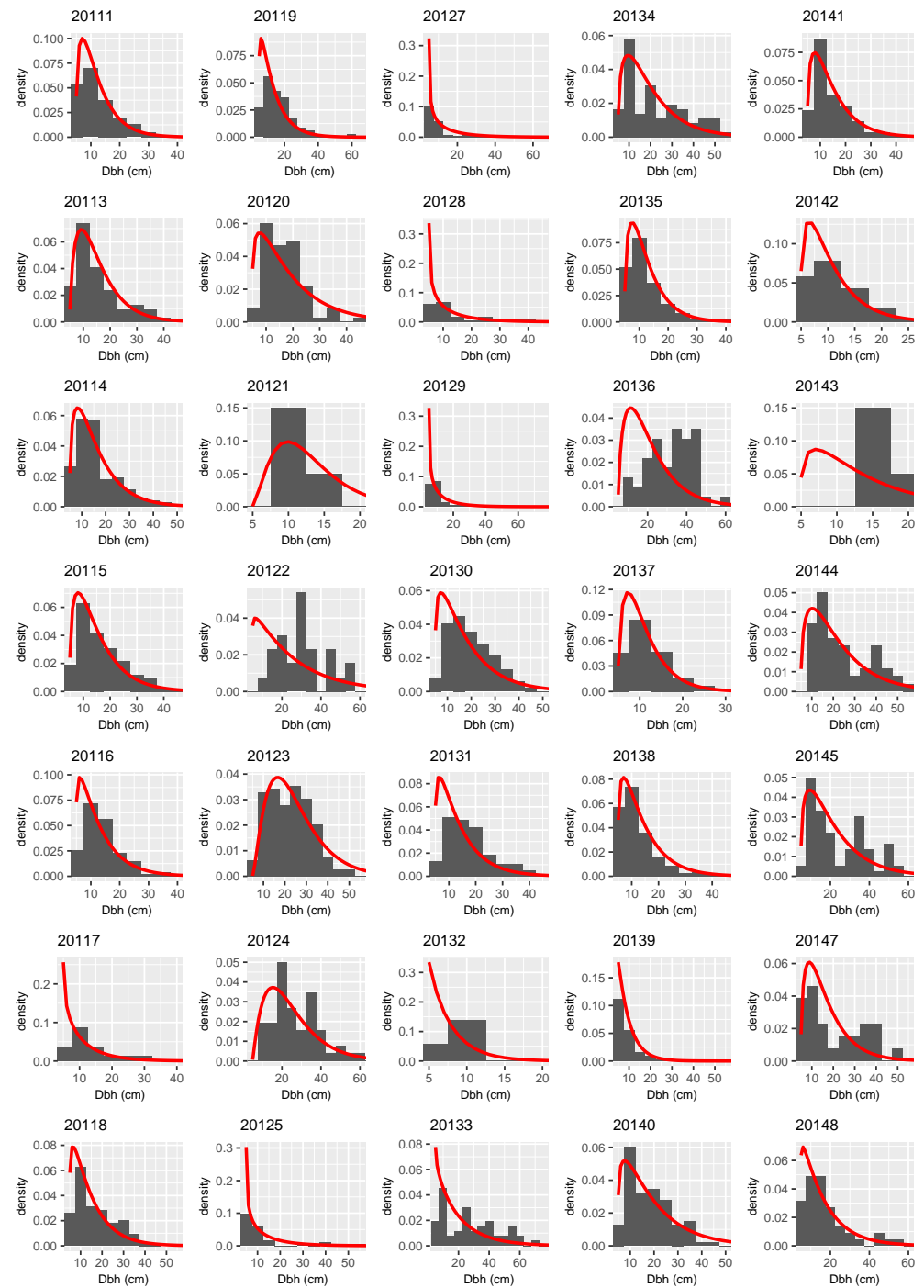
Figure A4. Histograms (grey bars) and posterior predictive distributions (red curves) of the DBH at the sample plots (plot id in title).
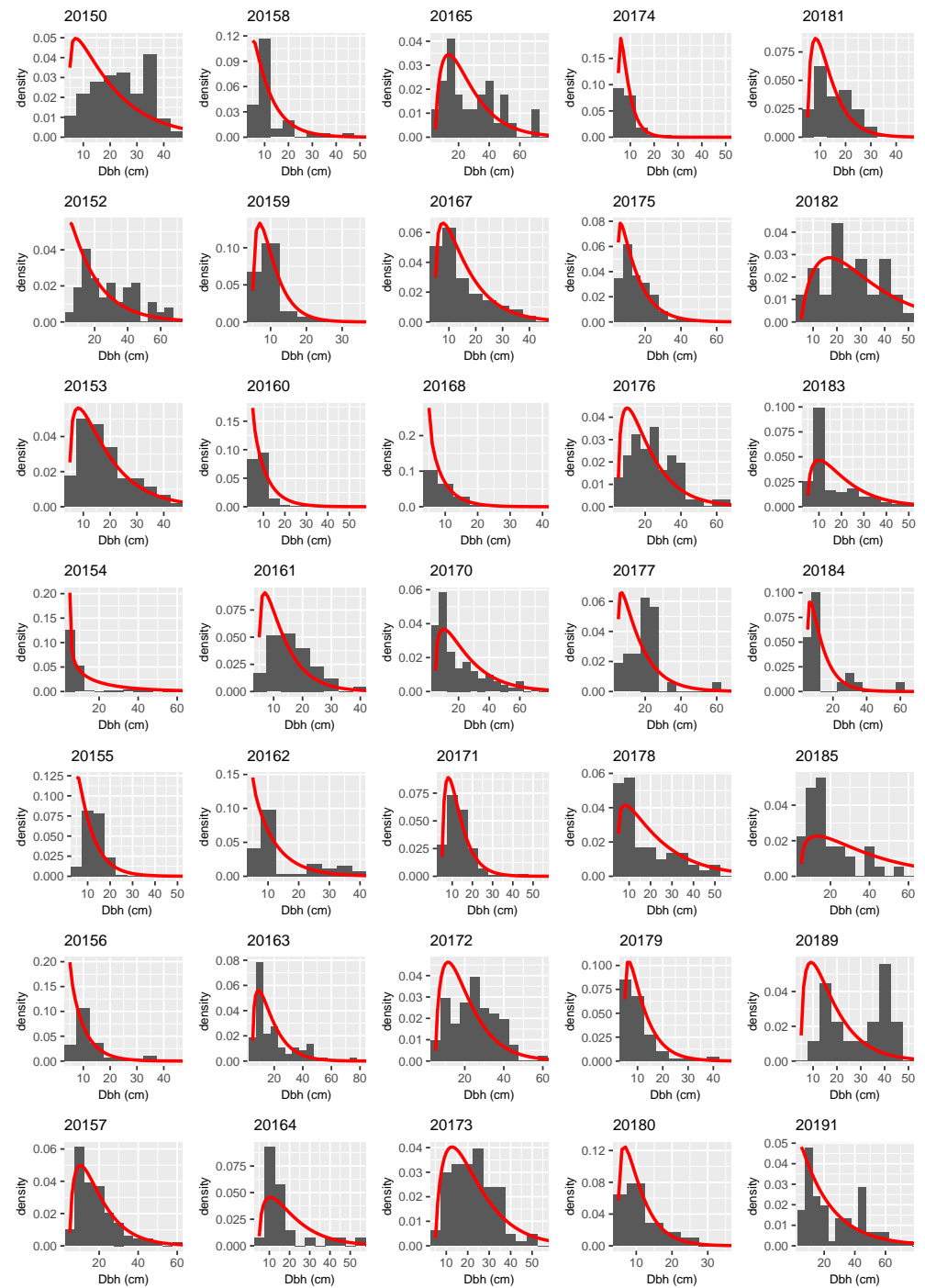
Figure A5. Histograms (grey bars) and posterior predictive distributions (red curves) of the DBH at the sample plots (plot id in title).
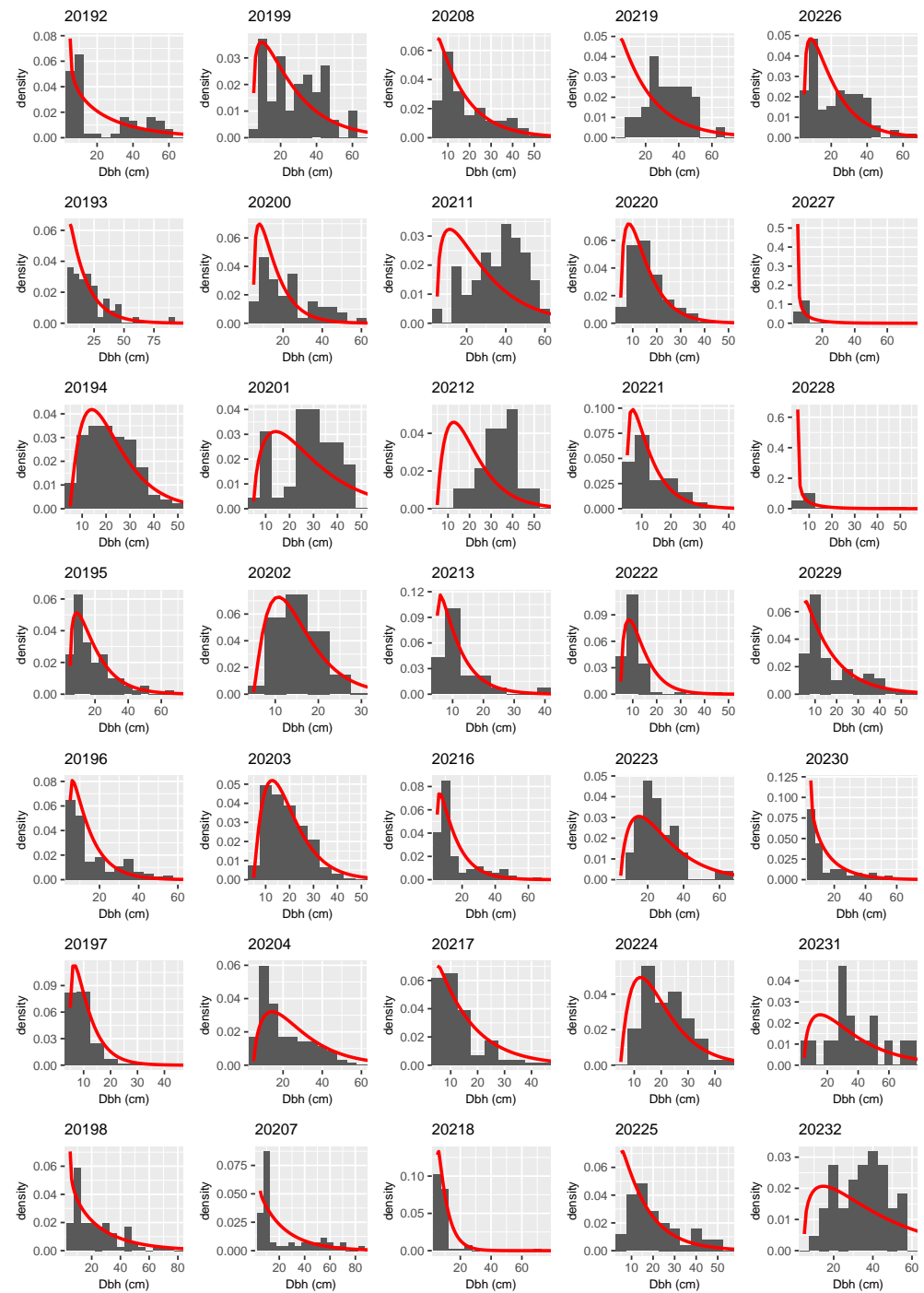
Figure A6. Histograms (grey bars) and posterior predictive distributions (red curves) of the DBH at the sample plots (plot id in title).
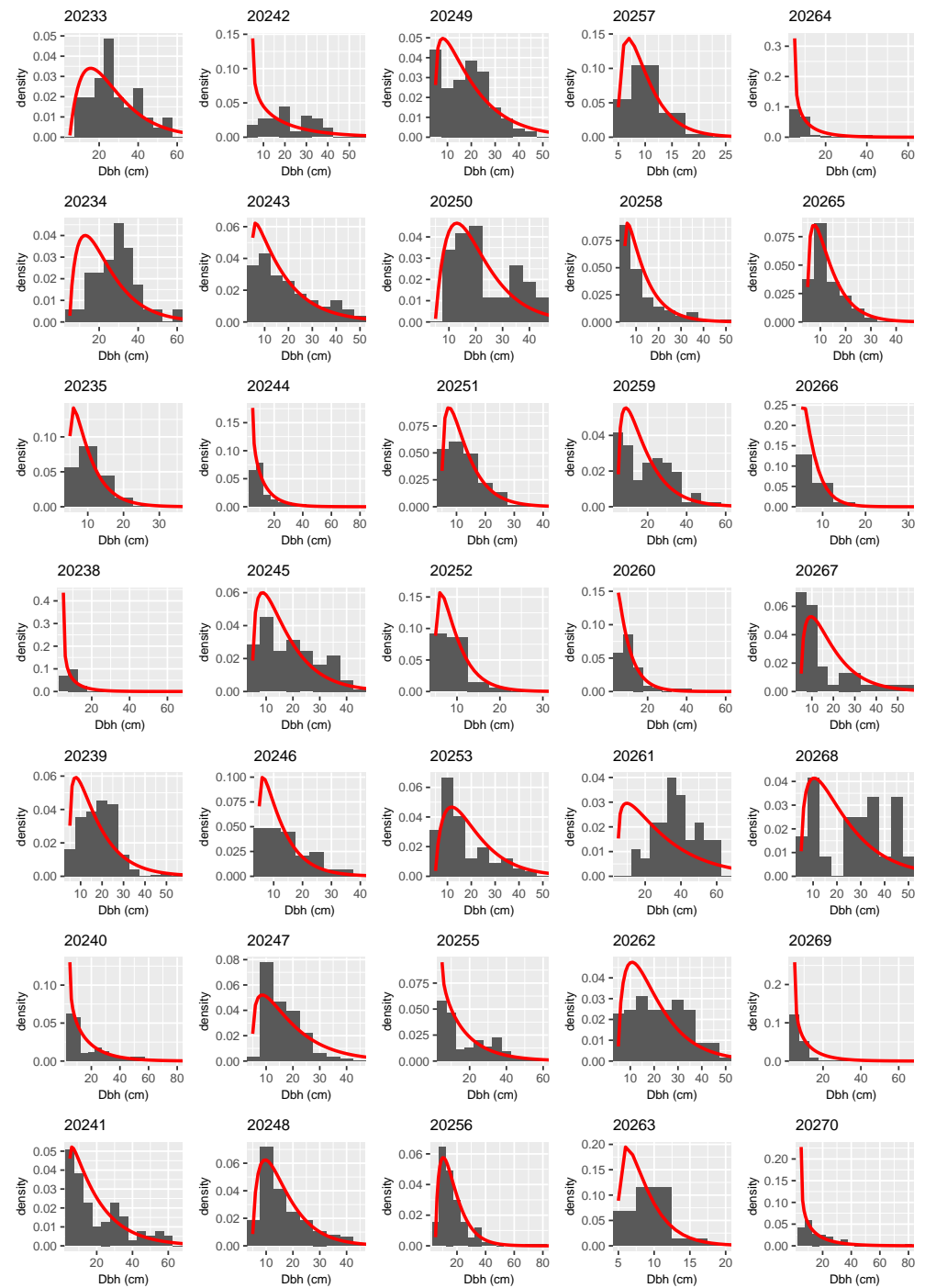
Figure A7. Histograms (grey bars) and posterior predictive distributions (red curves) of the DBH at the sample plots (plot id in title).
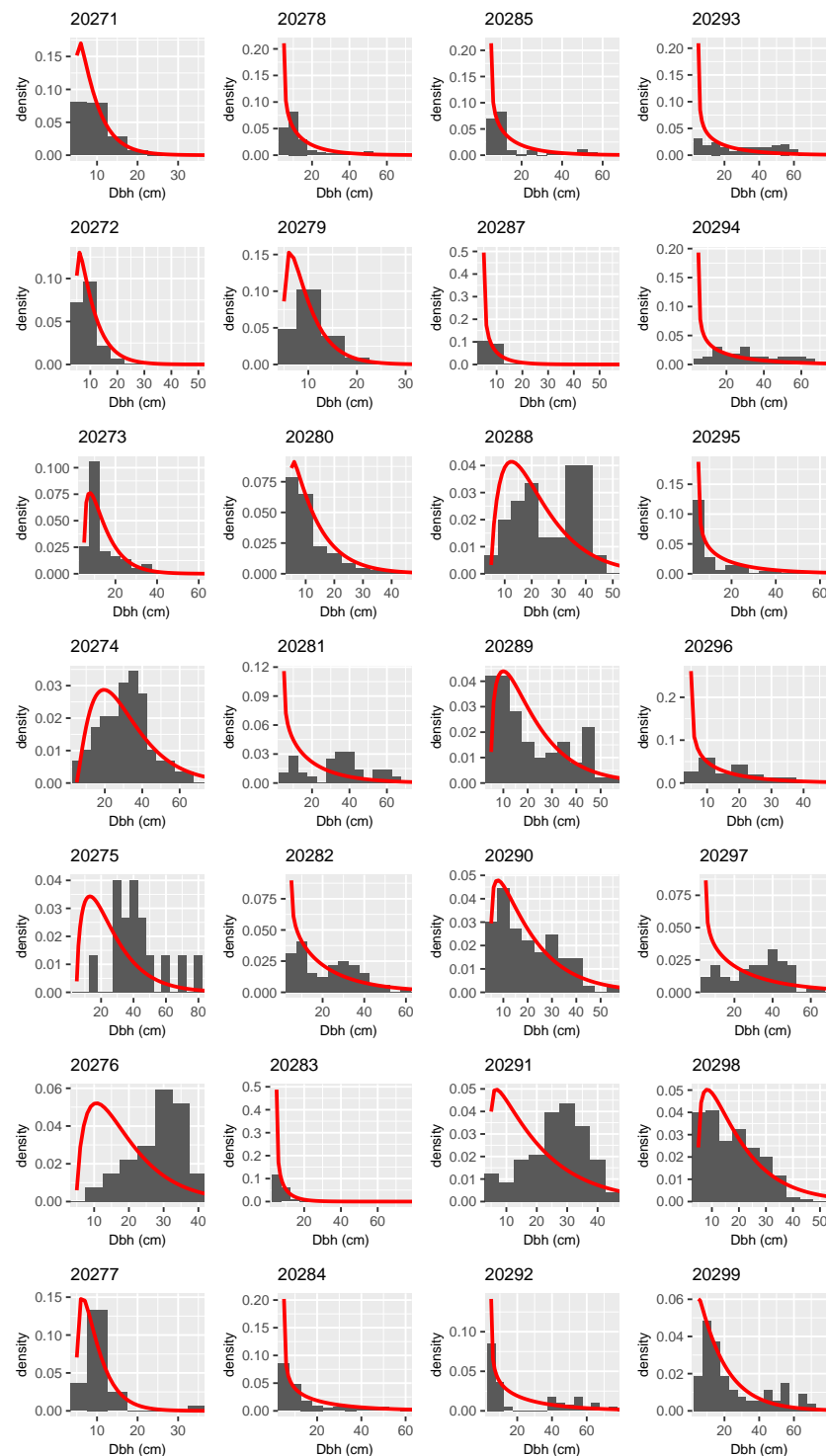
Figure A8. Histograms (grey bars) and posterior predictive distributions (red curves) of the DBH at the sample plots (plot id in title).

References

1. Brang, P. Resistance and elasticity: Promising concepts for the management of protection forests in the European Alps. *For. Ecol. Manag.* **2001**, *145*, 107–119. [CrossRef]
2. Perzl, F.; Huber, A.; Fromm, R.; Hagen, K.; Rössel, M.; Outer, J.D. Wald mit Steinschlag-Objektschutzfunktion in Österreich. *Bedeut. Und Herausforderung. Bfw-Praxisinformation* **2017**, *45*, 8–12.

3. BML Zahlen und Fakten 2022. Booklet, Österreichisches Bundesministerium für Land- und Forstwirtschaft, Regionen und Wasserwirtschaft, Abt. Präs. 5 sowie Fachsektionen und Fachabteilungen des BML, Wien. 2022. Available online: https://info.bml.gv.at/dam/jcr:d108c97d-0e16-42fc-92fb-360280464006/BML_Broschuere_Zahlen_und_Fakten_DE_2022_Barrierefrei%20(002).pdf (accessed on 10 June 2024).

4. Dorren, L.K.; Berger, F.; le Hir, C.; Mermin, E.; Tardif, P. Mechanisms, effects and management implications of rockfall in forests. *For. Ecol. Manag.* **2005**, *215*, 183–195. [CrossRef]

5. Teich, M.; Bebi, P. Evaluating the benefit of avalanche protection forest with GIS-based risk analyses—A case study in Switzerland. *For. Ecol. Manag.* **2009**, *257*, 1910–1919. [CrossRef]

6. Bebi, P.; Kienast, F.; Schönenberger, W. Assessing structures in mountain forests as a basis for investigating the forests' dynamics and protective function. *For. Ecol. Manag.* **2001**, *145*, 3–14. [CrossRef]

7. Köhl, M.; Magnussen, S.; Marchetti, M. *Sampling Methods, Remote Sensing and GIS Multiresource Forest Inventory*; Springer: Berlin/Heidelberg, Germany, 2006. [CrossRef]

8. Adnan, S.; Maltamo, M.; Coomes, D.A.; García-Abril, A.; Malhi, Y.; Manzanera, J.A.; Butt, N.; Morecroft, M.; Valbuena, R. A simple approach to forest structure classification using airborne laser scanning that can be adopted across bioregions. *For. Ecol. Manag.* **2019**, *433*, 111–121. [CrossRef]

9. Yao, W.; Krzystek, P.; Heurich, M. Tree species classification and estimation of stem volume and DBH based on single tree extraction by exploiting airborne full-waveform LiDAR data. *Remote Sens. Environ.* **2012**, *123*, 368–380. [CrossRef]

10. Schütz, J.P. Silvicultural tools to develop irregular and diverse forest structures. *For. Int. J. For. Res.* **2002**, *75*, 329–337. [CrossRef]

11. D'Amato, A.W.; Bradford, J.B.; Fraver, S.; Palik, B.J. Forest management for mitigation and adaptation to climate change: Insights from long-term silviculture experiments. *For. Ecol. Manag.* **2011**, *262*, 803–816. [CrossRef]

12. Gough, C.M.; Atkins, J.W.; Fahey, R.T.; Hardiman, B.S. High rates of primary production in structurally complex forests. *Ecology* **2019**, *100*, e02864, [CrossRef] [PubMed]

13. Schütz, J.P. Opportunities and strategies of transforming regular forests to irregular forests. *For. Ecol. Manag.* **2001**, *151*, 87–94. [CrossRef]

14. Morgenroth, J.; Nowak, D.J.; Koeser, A.K. DBH Distributions in America's Urban Forests—An Overview of Structural Diversity. *Forests* **2020**, *11*, 135. [CrossRef]

15. Hyink, D.M.; Moser, J.W. A Generalized Framework for Projecting Forest Yield and Stand Structure Using Diameter Distributions. *For. Sci.* **1983**, *29*, 85–95. [CrossRef]

16. Knoebel, B.R.; Burkhart, H.E. A Bivariate Distribution Approach to Modeling Forest Diameter Distributions at Two Points in Time. *Biometrics* **1991**, *47*, 241–253. [CrossRef]

17. Finley, A.O.; Banerjee, S.; Weiskittel, A.R.; Babcock, C.; Cook, B.D. Dynamic spatial regression models for space-varying forest stand tables. *Environmetrics* **2014**, *25*, 596–609. [CrossRef]

18. Rigby, R.A.; Stasinopoulos, D.M. Generalized additive models for location, scale and shape. *J. R. Stat. Soc. Ser.* **2005**, *54*, 507–554. [CrossRef]

19. Klein, N.; Kneib, T.; Lang, S.; Sohn, A. Bayesian structured additive distributional regression with an application to regional income inequality in Germany. *Ann. Appl. Stat.* **2015**, *9*, 1024–1052. [CrossRef]

20. Klein, N.; Kneib, T.; Lang, S. Bayesian Generalized Additive Models for Location, Scale, and Shape for Zero-Inflated and Overdispersed Count Data. *J. Am. Stat. Assoc.* **2015**, *110*, 405–419. [CrossRef]

21. Klein, N.; Kneib, T.; Klasen, S.; Lang, S. Bayesian structured additive distributional regression for multivariate responses. *J. R. Stat. Soc. Ser.* **2015**, *64*, 569–591. [CrossRef]

22. Umlauf, N.; Klein, N.; Zeileis, A. BAMLSS: Bayesian Additive Models for Location, Scale and Shape (and Beyond). *J. Comput. Graph. Stat.* **2018**, *27*, 612–627. [CrossRef]

23. Umlauf, N.; Klein, N.; Simon, T.; Zeileis, A. bamlss: A Lego Toolbox for Flexible Bayesian Regression (and Beyond). *J. Stat. Softw.* **2021**, *100*, 1–53. [CrossRef]

24. Kneib, T.; Silbersdorff, A.; Säfken, B. Rage Against the Mean—A Review of Distributional Regression Approaches. *Econom. Stat.* **2023**, *26*, 99–123. [CrossRef]

25. Gollob, C.; Ritter, T.; Wassermann, C.; Nothdurft, A. Influence of Scanner Position and Plot Size on the Accuracy of Tree Detection and Diameter Estimation Using Terrestrial Laser Scanning on Forest Inventory Plots. *Remote Sens.* **2019**, *11*, 1602. [CrossRef]

26. Gollob, C.; Ritter, T.; Nothdurft, A. Forest Inventory with Long Range and High-Speed Personal Laser Scanning (PLS) and Simultaneous Localization and Mapping (SLAM) Technology. *Remote Sens.* **2020**, *12*, 1509. [CrossRef]

27. Tockner, A.; Gollob, C.; Kraßnitzer, R.; Ritter, T.; Nothdurft, A. Automatic tree crown segmentation using dense forest point clouds from Personal Laser Scanning (PLS). *Int. J. Appl. Earth Obs. Geoinf.* **2022**, *114*, 103025. [CrossRef]

28. Ritter, T.; Schwarz, M.; Tockner, A.; Leisch, F.; Nothdurft, A. Automatic Mapping of Forest Stands Based on Three-Dimensional Point Clouds Derived from Terrestrial Laser-Scanning. *Forests* **2017**, *8*, 265. [CrossRef]

29. Ritter, T.; Gollob, C.; Nothdurft, A. Towards an Optimization of Sample Plot Size and Scanner Position Layout for Terrestrial Laser Scanning in Multi-Scan Mode. *Forests* **2020**, *11*, 1099. [CrossRef]

30. Pollanschütz, J. Eine neue Methode der Formzahl- und Massenbestimmung stehender Stämme-Neue Form-bzw. Kubierungsfunkionen und ihre Anwendung—A new method for the estimation of stem forms. Technical Report 68, Forstliche Bundesversuchsanstalt Mariabrunn, 1965.

31. Land Oberösterreich. Digital Surface Model 40704. Available online: https://e-gov.ooe.gv.at/at.gv.ooe.intramapgem/dop/downloads/40704/40704_DOM_tif.zip (accessed on 7 August 2023).

32. Land Oberösterreich. Digital Terrain Model 40704. Available online: https://e-gov.ooe.gv.at/at.gv.ooe.intramapgem/dop/downloads/40704/40704_DGM_tif.zip (accessed on 7 August 2023).

33. Stasinopoulos, R.R.M.; Heller, G.; Bastiani, F.D. *Distributions for Modeling Location, Scale, and Shape: Using GAMLSS in R*; Chapman & Hall/CRC: Boca Raton, FL, USA, 2019.

34. Wood, S.N. Thin Plate Regression Splines. *J. R. Stat. Soc. Ser. Stat. Methodol.* **2003**, *65*, 95–114. [CrossRef]

35. Kammann, E.E.; Wand, M.P. Geoadditive Models. *J. R. Stat. Soc. Ser. Appl. Stat.* **2003**, *52*, 1–18. [CrossRef]

36. Spiegelhalter, D.J.; Best, N.G.; Carlin, B.P.; Van Der Linde, A. Bayesian Measures of Model Complexity and Fit. *J. R. Stat. Soc. Ser.* **2002**, *64*, 583–639. [CrossRef]

37. Gelman, A.; Hwang, J.; Vehtari, A. Understanding predictive information criteria for Bayesian models. *Stat. Comput.* **2014**, *24*, 997–1016. [CrossRef]

38. Zhou, R.; Wu, D.; Zhou, R.; Fang, L.; Zheng, X.; Lou, X. Estimation of DBH at Forest Stand Level Based on Multi-Parameters and Generalized Regression Neural Network. *Forests* **2019**, *10*, 778. [CrossRef]

39. Nothdurft, A.; Gollob, C.; Kraßnitzer, R.; Erber, G.; Ritter, T.; Stampfer, K.; Finley, A.O. Estimating timber volume loss due to storm damage in Carinthia, Austria, using ALS/TLS and spatial regression models. *For. Ecol. Manag.* **2021**, *502*, 119714. [CrossRef]

40. Roussel, J.R.; Auty, D.; Coops, N.C.; Tompalski, P.; Goodbody, T.R.; Meador, A.S.; Bourdon, J.F.; de Boissieu, F.; Achim, A. lidR: An R package for analysis of Airborne Laser Scanning (ALS) data. *Remote Sens. Environ.* **2020**, *251*, 112061. [CrossRef]

41. Roussel, J.R.; Auty, D. R Package, version 4.0.4. Airborne LiDAR Data Manipulation and Visualization for Forestry Applications. 2023. Available online: https://cran.r-project.org/package=lidR (accessed on 9 June 2024).